

Supporting information

Twin-like chiral configuration of calcium oxalate monohydrate mesocrystal regulated with organic framework in grape leaves

Ryosuke Tanaka, Hiroto Watanabe, Yuya Oaki, and Hiroaki Imai*

Department of Applied Chemistry, Faculty of Science and Technology, Keio University

3-14-1 Hiyoshi, Kohoku-ku, Yokohama 223-8522, Japan.

**E-mail: hiroaki@aplc.keio.ac.jp*

Fig. S1 A photo of a grape leaf, optical micrographs of idioblasts in a leaf, and SEM images of a cross section of a leaf.

Fig. S2 SEM images and a schematic illustration of a bundle of raphides.

Fig. S3. XRD pattern and Raman spectra of raphide bundles and standard COM.

Fig. S4 SEM images of a raphide after dissolution of COM with EDTA solution and after removal of organic matter with calcination.

Fig. S5 FTIR spectra of raphide bundles and standard COM.

Fig. S6 TEM images and SAED patterns of raphides, and TEM and SEM images and schematic illustration of the same raphide shown in Fig. 5d in the main text.

Fig. S7 Optical micrographs and schematic illustrations indicating variation of morphology of raphide bundles.

Fig. S8 An SEM image of a bundle of raphides after demineralization and TEM and SEM images of longitudinal sections of immature raphides.

Fig. S9 TEM and enlarged SEM images of lateral sections of immature raphides.

Fig. S10 Optical micrographs of a bundle before and after decomposition into needles by a weak mechanical stimulation after removal of cytoplasm.

Table S1 FTIR assignments of COM and protein in raphides and cellulose in Fig. S2

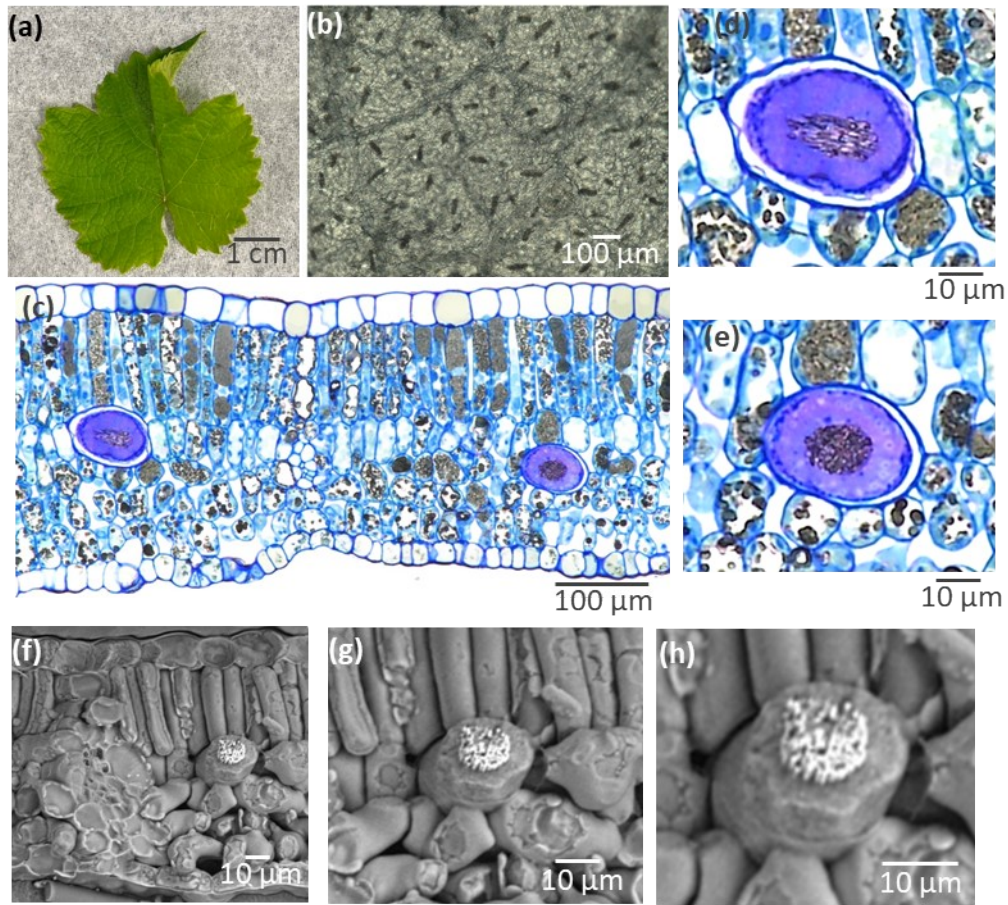


Fig. S1 A photo (a) of a grape leaf, optical micrographs of idioblasts in a leaf (b–e), and SEM images of a cross section of a leaf (f–h). A plan-view image of a bleached sample (b) and cross-sectional images of a stained sample (c–e) and a quickly frozen sample (f–h). A longitudinal section (d) and lateral sections (c, e–h) of idioblasts.

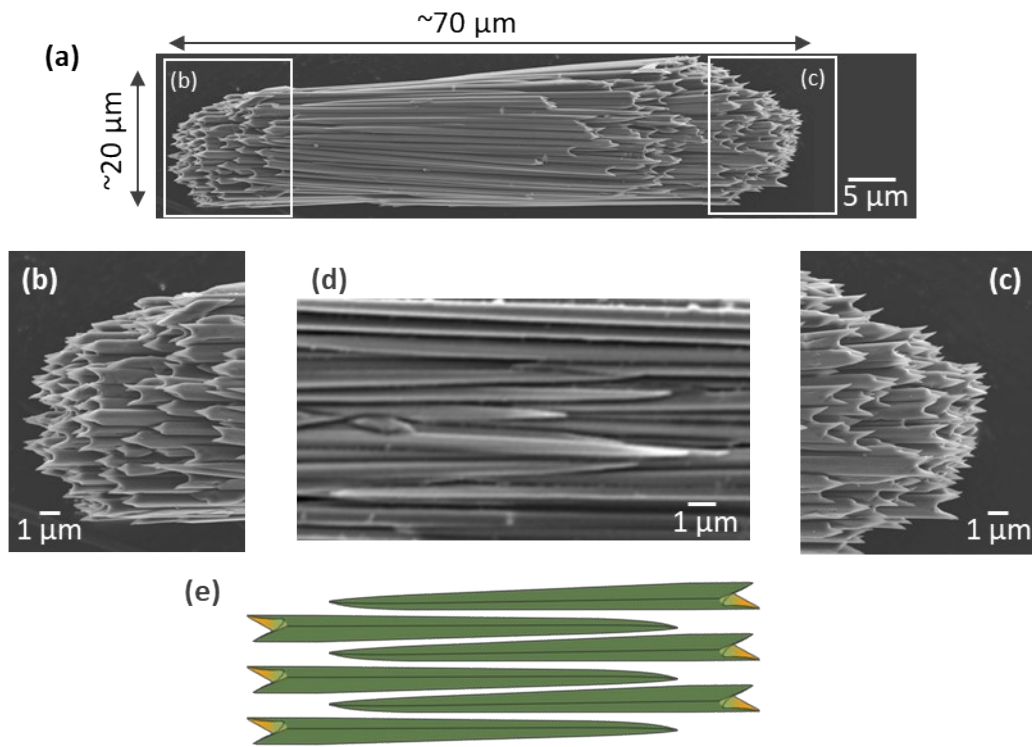


Fig. S2 SEM images (a–d) and a schematic illustration (e) of a bundle of raphides. A whole body (a), both ends (b, c), and the inside (d) of a bundle.

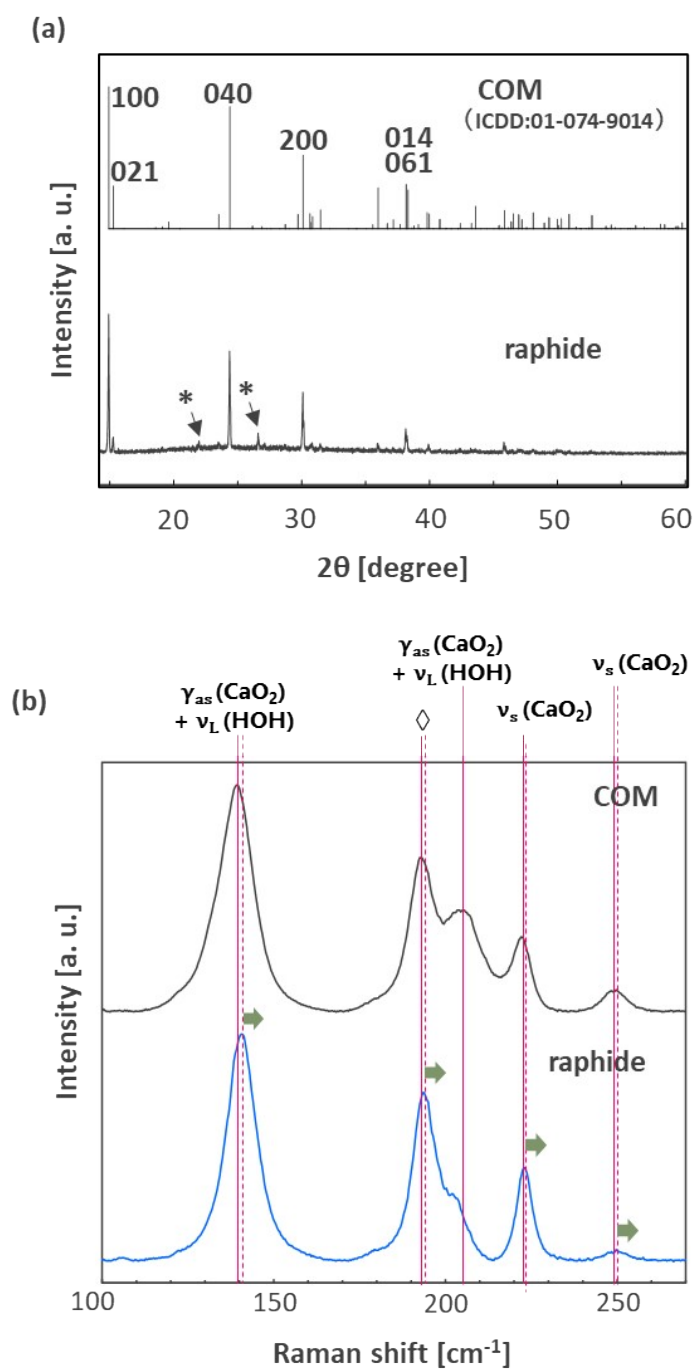


Fig. S3 A typical XRD pattern (a) and Raman spectra in a low wavenumber region (b) of raphide bundles and standard COM. Diffraction peaks of raphides were almost consistent with ICDD of COM/whewellite (monoclinic, $P2_1/c$) with several unknown peaks. Raman peaks are attributed to the lattice modes, although the peak (\diamond) around 193 cm^{-1} has not been assigned to a specific vibration.¹ Slight variations in the Raman signals between raphides and standard COM suggest the presence of distortion of the crystal lattice in the biogenic product. *: unknown peaks, γ_{as} : twisting (out-of-plane bending) mode, ν_L : libration mode, ν_s : symmetric stretching mode

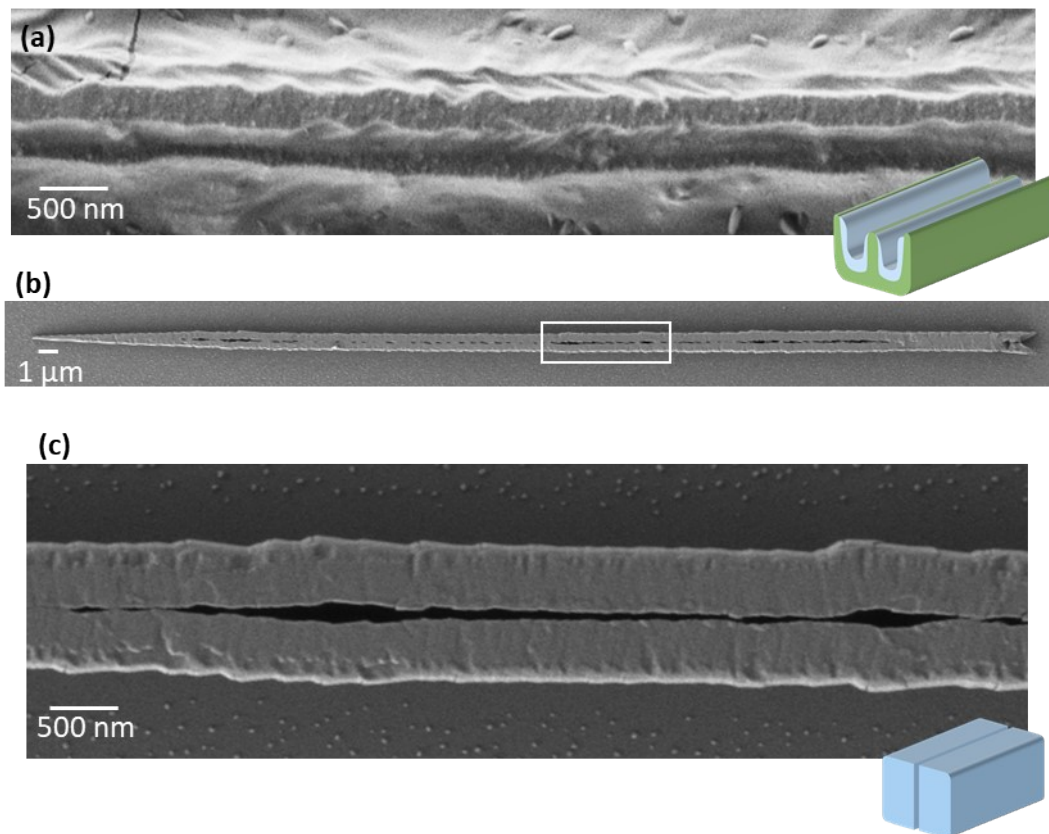


Fig. S4 SEM images with schematic illustrations of a raphide after dissolution of COM with EDTA solution (a) and after removal of organic matter with calcination at 340°C in air (b, c).

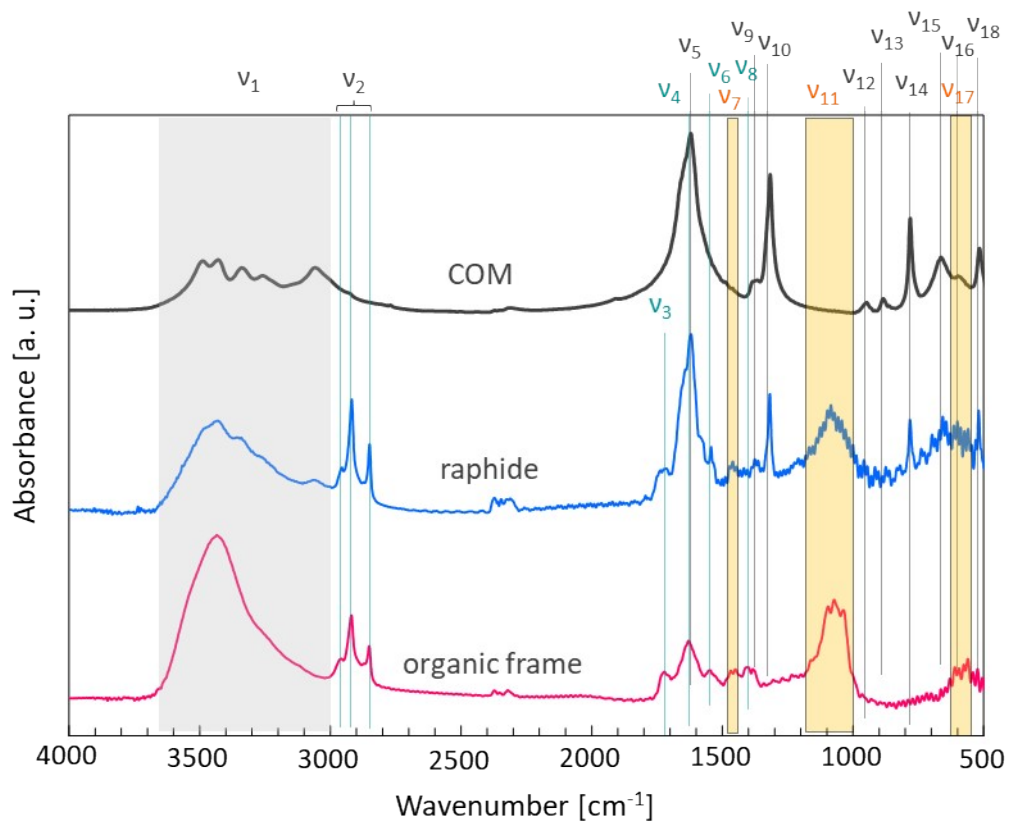


Fig. S5 FTIR spectra of raphide bundles, standard COM and organic frames.

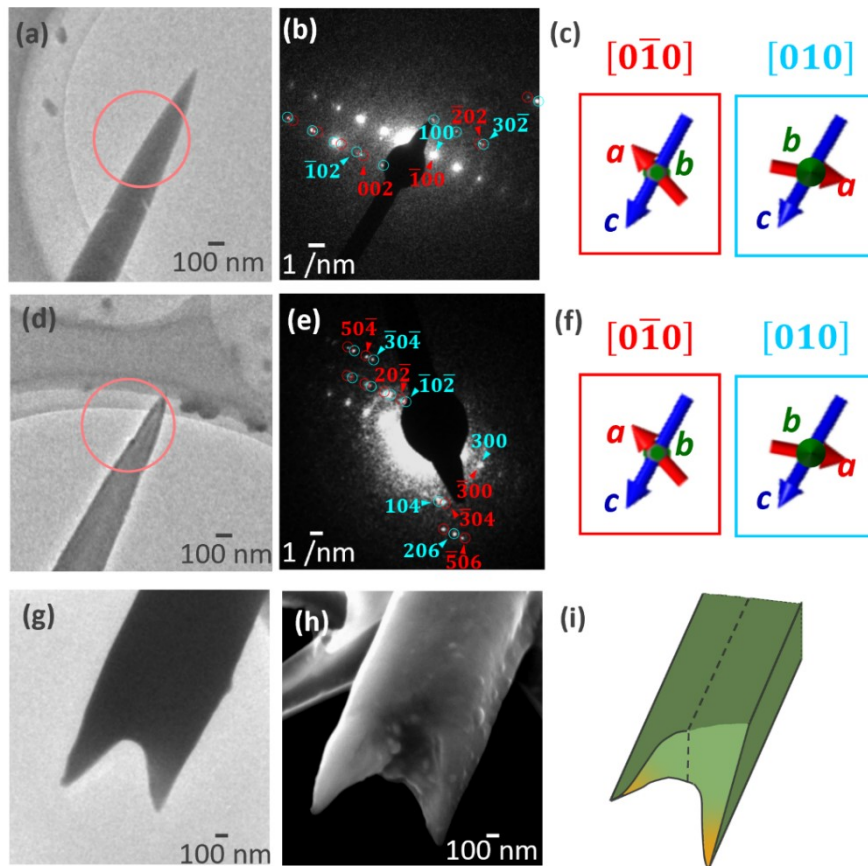


Fig. S6 TEM images (a, d), SAED patterns (b, e), crystallographic directions (c, f) of the pointed tips of raphides, and TEM (g) and SEM (h) images and schematic illustrations (i) of the two tails of a raphide. The TEM image (g) is the same as Fig. 5d. The SEM image (h) indicates that the left and right tails are located at the upper and lower sides, respectively, as shown in (i). The center wall is shown as a vertical line (i).

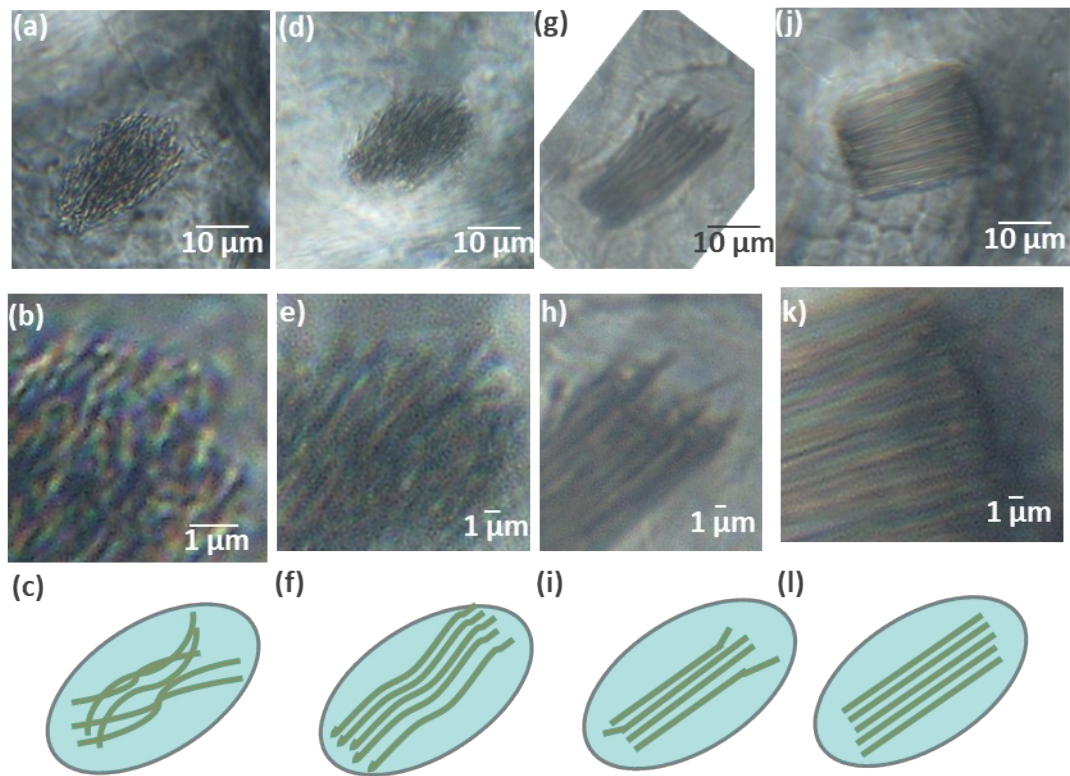


Fig. S7 Optical micrographs (a–k) and schematic illustrations (c, f, i, k) indicating variation of morphology of raphide bundles with growth in a leaf. Enlarged views (a, d, g, j) of raphide bundles shown in (b, e, h, k), respectively.

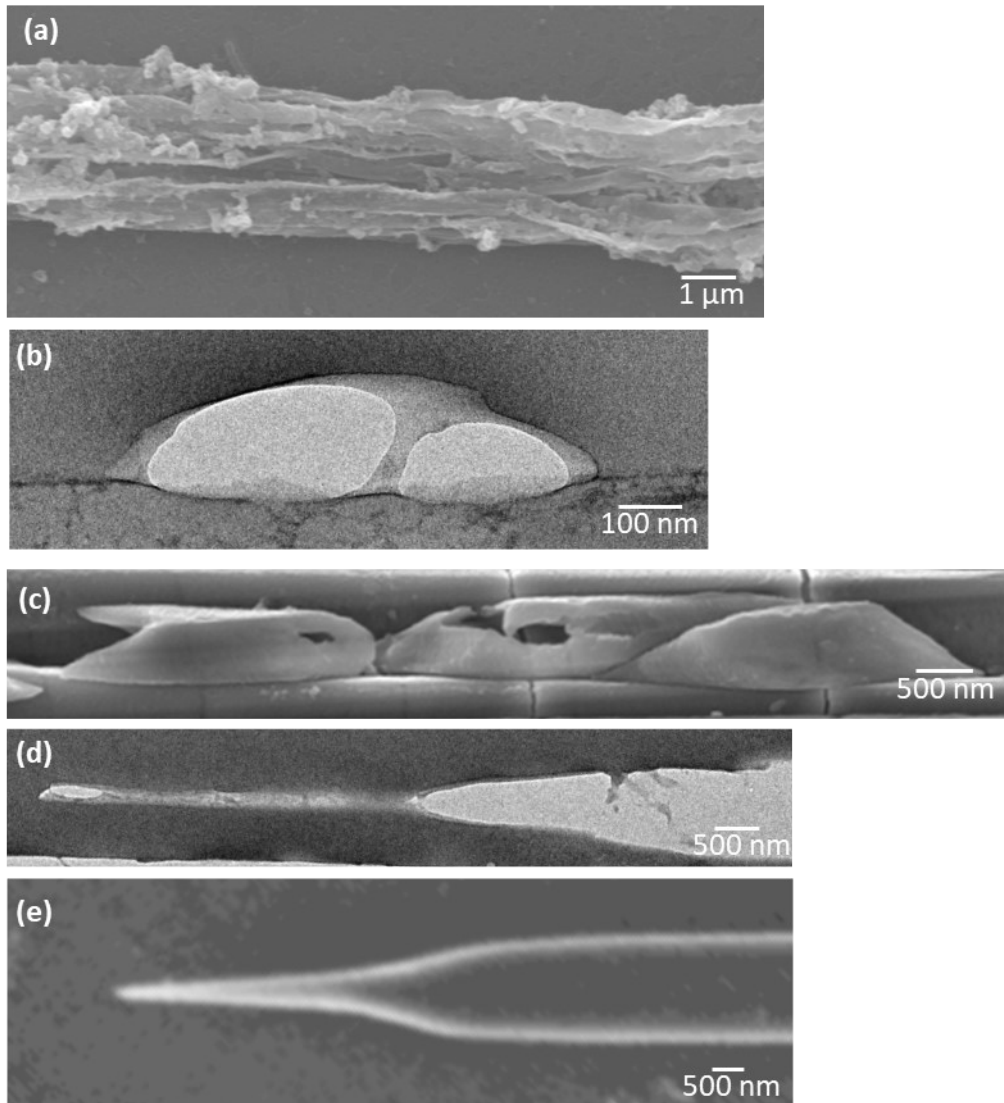


Fig. S8 An SEM image of a bundle of raphides after demineralization with EDTA (a). TEM (b, d) and SEM (c, e) images of longitudinal sections in the organic framework (b, d) and side views (c, e) of immature raphides.

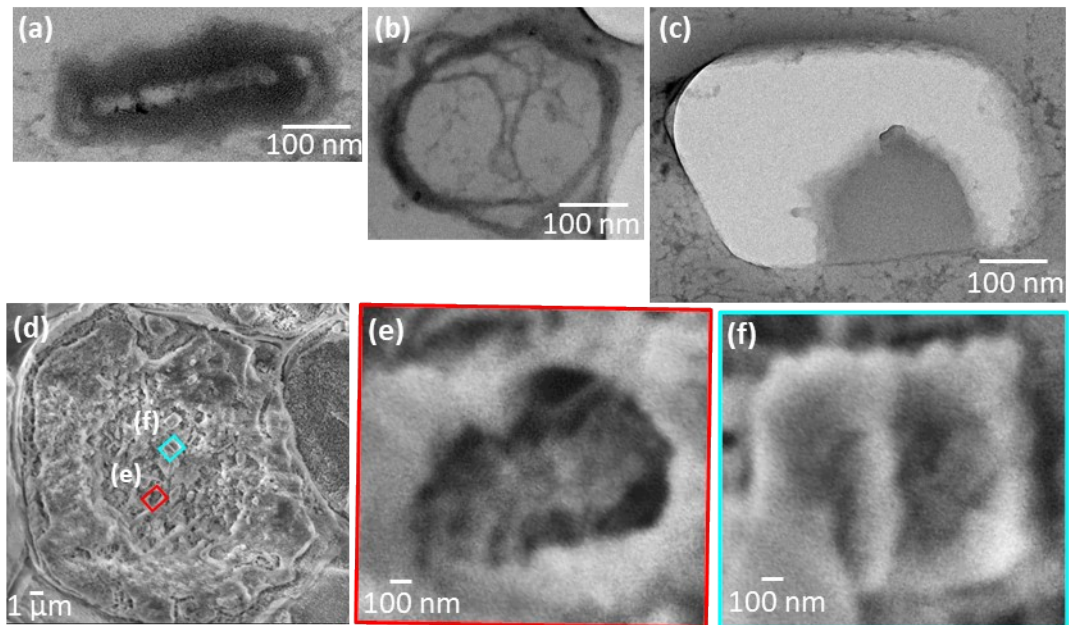


Fig. S9 TEM (a–c) and enlarged SEM (e, f) images of lateral sections of immature raphides. Organic frames without crystal (a, b) and with partially deposited crystal (c, e, f). A cross-sectional SEM image of an idioblast (d).

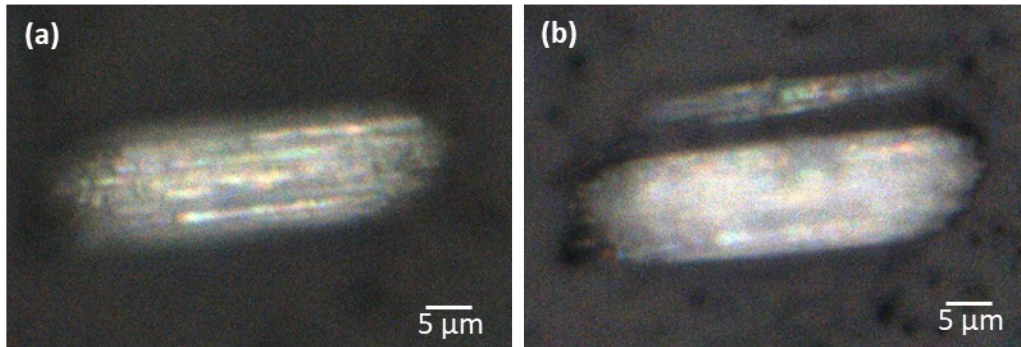


Fig. S10 Optical micrographs of a bundle before (a) and after (b) decomposition into needles by a weak mechanical stimulation after removal of cytoplasm. A tungsten needle of a micromanipulator was used to provide weak mechanical stimulation to the raphide bundle.

Table S1 FTIR assignments of COM and protein in raphides and cellulose in Fig. S2.¹⁻³

ν_i	Assignments
ν_1	O-H stretching of COM, protein, or/ and cellulose
ν_2	C-H stretching of protein or/and cellulose
ν_3	C=O stretching of lipid
ν_4	Amide I
ν_5	C=O asymmetric stretching of COM
ν_6	Amide II
ν_7	Scissoring C-H of cellulose
ν_8	C=O symmetric stretching of COO ⁻ side chains in protein
ν_9	C=O symmetric stretching of COM
ν_{10}	C=O symmetric stretching of COM
ν_{11}	C-O-C of Glycoside bond asymmetric stretching Glucose ring stretching C-O stretching of cellulose
ν_{12}	H-O-H libration of COM
ν_{13}	C-C stretching and H-O-H libration of COM
ν_{14}	O-C-O bending of COM
ν_{15}	H-O-H libration and bending of COM
ν_{16}	H-O-H libration and bending of COM
ν_{17}	C-OH bending of cellulose C-O stretching of cellulose
ν_{18}	C-C stretchig of COM

References

- 1 I. Petit, G. D. Belletti, T. Debroise, M. J. Llansola-Portoles, I. T. Lucas, C. Leroy, C. Bonhomme, L. Bonhomme-Coury, D. Bazin, M. Daudon, E. Letavernier, J. P. Haymann, V. Frochot, F. Babonneau, P. Quaino and F. Tielens, *ChemistrySelect*, 2018, **3**, 8801–8812.
- 2 X. Li, W. Zhang, J. Lu, L. Huang, D. Nan, M. A. Webb, F. Hillion and L. Wang, *Chem. Mater.*, 2014, **26**, 3862–3869.
- 3 M. Schwanninger, J. C. Rodrigues, H. Pereira and B. Hinterstoisser, *Vib. Spectrosc.*, 2004, **36**, 23–40.